

---

# CMS Physics Analysis Summary

---

Contact: cms-pag-conveners-susy@cern.ch

2012/11/16

## Search for supersymmetry in final states with missing transverse energy and 0, 1, 2, 3, or $\geq 4$ b-quark jets in 8 TeV pp collisions using the variable $\alpha_T$

The CMS Collaboration

### Abstract

A search for supersymmetry in final states with jets and missing transverse energy is performed in pp collisions at a centre-of-mass energy of  $\sqrt{s} = 8$  TeV. The data sample corresponds to an integrated luminosity of  $11.7 \text{ fb}^{-1}$  collected by the CMS experiment at the LHC. In this search, a dimensionless kinematic variable,  $\alpha_T$ , is used as the main discriminator between events with genuine and misreconstructed missing transverse energy. The search is performed in a signal region that is binned according to the number of reconstructed jets, the scalar sum of the transverse energy of these jets, and the number of jets identified as originating from a bottom quark. No excess of events over the standard model expectation is found. Exclusion limits are set in the parameter space of simplified models, with a special emphasis on compressed spectra and third-generation scenarios.



## 1 Introduction

Supersymmetry (SUSY) is generally regarded as one of the most likely extensions to the Standard Model of particle physics (SM) [1–8]. It is a well-established theory based on the unique extension of the space-time symmetry group underpinning the SM, introducing a relationship between fermions and bosons. If the multiplicative quantum number R-parity is conserved [9], SUSY particles such as squarks and gluinos are produced in pairs and decay to the lightest SUSY particle (LSP), which is generally assumed to be a weakly interacting massive particle. Hence, a typical final-state signature is rich in jets and contains a significant amount of missing transverse energy ( $\cancel{E}_T$ ).

The search described below is therefore designed to be sensitive to missing transverse energy signatures in events with two or more energetic jets. The search follows closely that described in Ref. [10], which is in turn based on two previous inclusive searches [11, 12]. Events are categorised according to the scalar sum of the jet transverse energies and the number of jets originating from bottom quarks (b-quark jets). With respect to the previous search [10], two refinements are made: an additional b-quark jet multiplicity bin is added (requiring at least four b-quark jets), and events are further categorised according to the number of reconstructed jets per event (requiring two or three jets, or at least four jets). This approach improves the sensitivity to both gluino-induced and direct production of third-generation squark signatures, while maintaining an inclusive approach that provides sensitivity to the wide variety of SUSY event topologies that could arise from squark-squark, squark-gluino and gluino-gluino pair-production at the LHC. The results presented here are based on a data sample of pp collisions collected in 2012 at a centre-of-mass energy of 8 TeV, which corresponds to an integrated luminosity of  $11.7 \pm 0.5 \text{ fb}^{-1}$ .

In 2010 and 2011 the CMS and ATLAS experiments performed various searches [11–19] for the production of massive coloured sparticles and their subsequent decay to a final state of jets and missing transverse energy. These searches were performed with a dataset of pp collisions at  $\sqrt{s} = 7 \text{ TeV}$ , and no significant deviations from SM expectations were observed. The majority of these searches were interpreted in the context of a specific model of SUSY-breaking, the constrained minimal supersymmetric extension of the standard model (CMSSM) [20–22]. The simplifying assumption of universality at an energy scale of  $\mathcal{O}(10^{16}) \text{ GeV}$  makes the CMSSM a useful framework to study SUSY phenomenology at colliders, and to benchmark the performance of experimental searches. However, these universality conditions result in significant restrictions on the possible SUSY particle mass spectra. For example, the CMSSM prevents the realisation of compressed mass spectra, where the mass difference between the initially produced squark or gluino and the LSP is small.

Alternatively, simplified models [23–26] can be used to interpret the search results presented below. Each model is characterised by a single production and decay mode involving a limited set of SUSY and SM particles. These models allow comprehensive studies of individual SUSY event topologies, which are performed in a two-dimensional parameter space of different sparticle masses and mass splittings.

## 2 The CMS apparatus

The central feature of the CMS detector is a superconducting solenoid, which provides an axial magnetic field of 3.8 T. The bore of the solenoid is instrumented with several particle detection systems. Silicon pixel and strip tracking systems measure charged particle trajectories with full azimuthal ( $\phi$ ) coverage and a pseudorapidity acceptance of  $|\eta| < 2.5$ , where  $\eta \equiv -\ln[\tan(\theta/2)]$

and  $\theta$  is the polar angle with respect to the counterclockwise beam direction. The resolutions on the transverse momentum and impact parameter of a charged particle with  $p_T < 40\text{ GeV}$  is typically 1% and 15  $\mu\text{m}$ , respectively. A lead tungstate crystal electromagnetic calorimeter (ECAL) and a brass/scintillator hadron calorimeter surround the tracking volume. The forward region is covered by an iron/quartz-fiber hadron calorimeter. The ECAL covers  $|\eta| < 3.0$  and provides an energy resolution of better than 0.5% for unconverted photons with transverse energies above 100 GeV. The hadron calorimeters cover  $|\eta| < 5.0$  with a resolution in jet energy,  $E$  (GeV), of about  $100\%/\sqrt{E}$ . Muons are identified in gas-ionization detectors, covering  $|\eta| < 2.4$ , embedded in the steel return yoke. The CMS detector is nearly hermetic, which allows for momentum-balance measurements in the plane transverse to the beam axis. A detailed description of the CMS detector can be found elsewhere [27].

### 3 Object definition

The offline selection criteria and event reconstruction follows the procedure described in [11, 12]. Jets are reconstructed from energy deposits in the calorimeter towers, clustered by the anti- $k_T$  algorithm [28] with a size parameter of 0.5. The raw jet energies measured by the calorimeter systems are corrected to remove the effects of overlapping pp collisions (pile-up) [29, 30], and to establish a uniform relative response in  $\eta$  and a calibrated absolute response in transverse momentum  $p_T$  [31]. Jets considered in the analysis are generally required to have transverse energy  $E_T > 50\text{ GeV}$ . Events are vetoed if any additional jet satisfies both  $E_T > 50\text{ GeV}$  and  $|\eta| > 3$ , or rare, spurious signals are identified in the calorimeters [32, 33]. The highest- $E_T$  jet is required to be within the central tracker acceptance ( $|\eta| < 2.5$ ) and the two highest- $E_T$  jets must each have  $E_T > 100\text{ GeV}$ . To suppress SM processes with genuine  $\cancel{E}_T$  from neutrinos, events containing an isolated electron [34] or muon [35] with  $p_T > 10\text{ GeV}$  are vetoed. To select a pure multijet topology, events are vetoed in which an isolated photon [36] with  $p_T > 25\text{ GeV}$  is found.

The presence of a b-quark jet is identified through a vertex that is displaced with respect to the primary interaction, using the combined secondary vertex algorithm [37] which incorporates several variables related to the vertex to build a discriminator between jets originating from bottom quarks and other sources. These include jets from c quarks and light-flavour quarks. Discriminator values above a certain threshold are used to tag jets as reconstructed b-quark jets. This threshold is chosen such that the mis-tagging rate, i.e. the probability to tag jets originating from light-flavour quarks as b-quark jets, is approximately 1% for jets with a transverse momenta of 80 GeV [37, 38]. This typically results in a b tagging efficiency, i.e. the probability to correctly tag jets originating from b quarks, in the range 60 – 70% [37, 38].

The following two variables characterize the visible energy and missing momentum in the transverse plane: the scalar sum of the transverse energy  $E_T$  of jets, defined as  $H_T = \sum_{i=1}^{N_{\text{jet}}} E_T$ , and the magnitude of the vector sum of the transverse momenta  $\vec{p}_T$  of jets, defined as  $\cancel{H}_T = |\sum_{i=1}^{N_{\text{jet}}} \vec{p}_T|$ , where  $N_{\text{jet}}$  is the number of jets with  $E_T > 50\text{ GeV}$ . Significant hadronic activity in the event is ensured by requiring  $H_T > 275\text{ GeV}$ . Following these selections, the background from multijet production, a manifestation of quantum chromodynamics (QCD), is still several orders of magnitude larger than the typical signal expected from SUSY.

## 4 Selection of multijet events with missing transverse energy

The  $\alpha_T$  kinematic variable, first introduced in Refs. [39–41], is used in the selection of multijet events to efficiently reject events either without significant  $\cancel{E}_T$  or with transverse energy mis-measurements, while retaining a large sensitivity to new physics with genuine  $\cancel{E}_T$  signatures. For dijet events, the  $\alpha_T$  variable is defined as:

$$\alpha_T = \frac{E_T^{j_2}}{M_T} \quad , \quad M_T = \sqrt{\left( \sum_{i=1}^2 E_T^{j_i} \right)^2 - \left( \sum_{i=1}^2 p_x^{j_i} \right)^2 - \left( \sum_{i=1}^2 p_y^{j_i} \right)^2} \quad (1)$$

where  $E_T^{j_2}$  is the transverse energy of the least energetic jet of the two, and  $M_T$  is the transverse mass of the dijet system. For a perfectly measured dijet event with  $E_T^{j_1} = E_T^{j_2}$  and jets back-to-back in  $\phi$ , and in the limit of large jet momenta compared to their masses, the value of  $\alpha_T$  is 0.5. In the case of an imbalance in the measured transverse energies of back-to-back jets,  $\alpha_T$  is smaller than 0.5. Values significantly greater than 0.5 are observed when the two jets are not back-to-back, recoiling against genuine  $\cancel{E}_T$ .

For events with three or more jets, an equivalent dijet system is formed by combining the jets in the event into two pseudo-jets. The  $E_T$  of each of the two pseudo-jets is calculated as the scalar sum of the measured  $E_T$  of the contributing jets. The combination chosen is the one that minimizes the  $E_T$  difference ( $\Delta H_T$ ) between the two pseudo-jets. This simple clustering criterion provides the best separation between multijet events and events with genuine  $\cancel{E}_T$ .

Events with extremely rare but large stochastic fluctuations in calorimetric measurements of jet energies can lead to values of  $\alpha_T$  slightly above 0.5. Such events are rejected by requiring  $\alpha_T > 0.55$ . A similar behaviour is observed in events with reconstruction failures, severe energy losses due to detector inefficiencies, or jets below the  $E_T$  threshold that result in significant  $H_T$  relative to the value of  $\cancel{E}_T$  (as measured by the calorimeter systems, which is not affected by jet  $E_T$  thresholds). These classes of events are rejected by applying dedicated vetoes, described further in Ref. [12]. The leakage above 0.5 becomes smaller with increasing  $H_T$ . This is due in part to increasing average jet energy and thus improving jet energy resolution. Further, the relative impact of jets falling below the  $E_T$  threshold is reduced as the scale of the event (i.e.  $H_T$ ) increases.

The signal region is defined by  $H_T > 275 \text{ GeV}$  and  $\alpha_T > 0.55$ , which is divided into eight bins in  $H_T$ : two bins of width 50 GeV in the range  $275 < H_T < 375 \text{ GeV}$ , five bins of width 100 GeV in the range  $375 < H_T < 875 \text{ GeV}$ , and a final open bin,  $H_T > 875 \text{ GeV}$ . As in Ref. [12], the jet  $E_T$  threshold is scaled down to 37 GeV and 43 GeV for the regions  $275 < H_T < 325 \text{ GeV}$  and  $325 < H_T < 375 \text{ GeV}$ , respectively. The highest- $E_T$  jet threshold is also scaled accordingly. This is done in order to maintain a background composition and event kinematics similar to those observed for the higher  $H_T$  bins. Candidate events are further categorised according to the number of jets per event,  $2 \leq n_{\text{jet}} \leq 3$  or  $n_{\text{jet}} \geq 4$ , and whether they contain exactly zero, one, two, three, or at least four reconstructed b-quark jets. For the category with at least four reconstructed b-quark jets, only three  $H_T$  bins are used:  $275 < H_T < 325 \text{ GeV}$ ,  $325 < H_T < 375 \text{ GeV}$  and  $H_T > 375 \text{ GeV}$ .

Events in the signal sample are recorded with multiple trigger conditions that must satisfy requirements on both  $H_T$  and  $\alpha_T$  in the range ( $H_T > 250 \text{ GeV}$  and  $\alpha_T > 0.55$ ) to ( $H_T > 400 \text{ GeV}$  and  $\alpha_T > 0.51$ ). The trigger efficiency is defined as the probability with which events that satisfy the signal sample selection criteria also satisfy the trigger conditions, and is measured from data separately for each  $n_{\text{jet}}$  multiplicity bin.

A disjoint hadronic control sample consisting predominantly of multijet events is defined by inverting the  $\alpha_T$  requirement for a given  $H_T$  region, which is used primarily in the estimation of any residual background from multijet events. These events are recorded by a set of  $H_T$  trigger conditions.

## 5 Background estimation from data

Once all selection requirements have been imposed, the contribution from multijet events is expected to be negligible. The remaining significant backgrounds in the hadronic signal region stem from SM processes with genuine  $\cancel{E}_T$  in the final state. In the case of events where no b-quark jets are identified, the largest backgrounds with genuine  $\cancel{E}_T$  arise from the production of W and Z bosons in association with jets, especially for  $2 \leq n_{\text{jet}} \leq 3$ . The weak decay  $Z \rightarrow \nu\bar{\nu}$  is the only relevant contribution from Z + jets events. For W + jets events, the two relevant sources are leptonic W decays, in which the lepton is not reconstructed or fails the isolation or acceptance requirements, and the weak decay  $W \rightarrow \tau\nu$  where the  $\tau$  decays hadronically and is identified as a jet. For events with one or more reconstructed b jets however, top quark production followed by semi-leptonic weak decays becomes the most important single background source, primarily for  $n_{\text{jet}} \geq 4$ . For events with only one reconstructed b-quark jet, the contribution of both W + jets and Z + jets backgrounds are of a similar size to the top background. For events with two reconstructed b-quark jets,  $t\bar{t}$  production dominates for  $n_{\text{jet}} \geq 4$ , while events with three or more reconstructed b-quark jets originate almost exclusively from  $t\bar{t}$  events, in which one or several jets are misidentified as b-quark jets.

In order to estimate the contributions from each of these backgrounds, three data control samples are used, which are binned in the same way as the signal sample. A  $\mu$  + jets data sample provides an estimate of the contributions from top quark and W production leading to W + jets final states. The remaining irreducible background of  $Z \rightarrow \nu\bar{\nu}$  + jets events in the hadronic signal region is estimated from both a data sample of  $Z \rightarrow \mu\mu$  + jets and  $\gamma$  + jets events, which share kinematic properties but have different acceptances. The  $Z \rightarrow \mu\mu$  + jets events have identical kinematic properties when the two muons are ignored, but a smaller branching ratio, while the  $\gamma$  + jets events have similar kinematic properties when the photon is ignored [42, 43], but a larger production cross section. The event selection criteria for the control samples are defined to ensure that any potential contamination from multijet events is negligible. Further, the selection also suppress signal contamination from a wide variety of SUSY models, including those considered in this analysis, to a negligible level.

### 5.1 Definition of data control samples

The  $\mu$  + jets sample is recorded using a trigger strategy which requires an isolated muon above a  $p_T$  threshold of 24 GeV and within  $|\eta| < 2.1$ . The event selection requires exactly one isolated muon that satisfies stringent quality criteria, with  $p_T > 30$  GeV and  $|\eta| < 2.1$ , in order for the trigger to be maximally efficient, around  $88.0 \pm 2.0$  %.

The transverse mass of the muon and  $\cancel{E}_T$  system must be larger than 30 GeV to ensure a sample rich in W bosons. The muon is required to be separated from the closest jet in the event by  $\Delta\eta$  and  $\Delta\phi$  such that the distance  $\Delta R \equiv \sqrt{\Delta\eta^2 + \Delta\phi^2} > 0.5$ . Further, the event is rejected if a second muon candidate is identified that does not satisfy all quality criteria or is non-isolated or is outside acceptance, and the two muon candidates have an invariant mass that is within a window of  $\pm 25$  GeV around the mass of the Z boson. No requirement on  $\alpha_T$  is made in order to increase the statistical precision of the predictions derived from this sample, while the impact of relaxing the  $\alpha_T$  requirement is tested with a dedicated set of closure tests described in Sec. 5.2.

The  $\mu\mu + \text{jets}$  sample follows the same trigger strategy and muon identification criteria as the  $\mu + \text{jets}$  sample, except that in the event selection criteria, the threshold for the muon with the lower  $p_T$  is 10 GeV. This leads to a trigger efficiency of  $95 \pm 2\%$  rising to  $98 \pm 2\%$  with increasing  $H_T$ . The event selection requires exactly two oppositely charged, isolated muons satisfying stringent quality criteria, and an invariant mass within a window of  $\pm 25$  GeV around the mass of the Z boson. Both muons are required to be separated from their closest jets in the event by the distance  $\Delta R > 0.5$ . Again, no requirement on  $\alpha_T$  is made.

The  $\gamma + \text{jets}$  sample is selected using a dedicated photon trigger condition requiring a localized, large energy deposit in the ECAL with  $E_T > 150$  GeV that satisfies loose photon identification and isolation criteria [36]. The offline selection requires  $H_T > 375$  GeV,  $\alpha_T > 0.55$ , and a single photon to be reconstructed with  $E_T > 165$  GeV,  $|\eta| < 1.45$ , satisfying tight isolation criteria, and with a minimum distance to any jet of  $\Delta R > 1.0$ . For these selection criteria, the photon trigger condition is found to be fully efficient.

## 5.2 Method for estimating genuine $E_T$ background

The method used to estimate the background contributions in the hadronic signal region relies on the use of translation factors, which are constructed per bin in the three dimensions of  $n_{\text{jet}}$ ,  $H_T$ , and the number of reconstructed b-quark jets per event,  $n_b^{\text{reco}}$ . Each factor, determined from simulation, is defined as the ratio of yields in a given bin of the hadronic signal sample ( $N_{\text{MC}}^{\text{signal}}$ ) and corresponding bin of the control sample ( $N_{\text{MC}}^{\text{control}}$ ). The factors are used to translate the observed yield measured in a control sample bin ( $N_{\text{obs}}^{\text{control}}$ ) into an expectation for the yield in the corresponding bin of the hadronic signal sample ( $N_{\text{pred}}^{\text{signal}}$ ):

$$N_{\text{pred}}^{\text{signal}}(n_{\text{jet}}, H_T, n_b^{\text{reco}}) = N_{\text{obs}}^{\text{control}}(n_{\text{jet}}, H_T, n_b^{\text{reco}}) \times \frac{N_{\text{MC}}^{\text{signal}}}{N_{\text{MC}}^{\text{control}}}(n_{\text{jet}}, H_T, n_b^{\text{reco}}). \quad (2)$$

The number of reconstructed b-quark jets per event ( $n_b^{\text{reco}}$ ) is estimated from a method based on truth-level information contained in the simulation, namely: the numbers of jets originating from underlying b quarks,  $n_b$ , and from light quarks,  $n_q$ , per event. All relevant combinations of  $n_b$  and  $n_q$  are considered, and event counts are recorded in bins of  $H_T$  for each combination,  $N(n_b, n_q)$ . The b tagging efficiency,  $\epsilon$ , and a flavour-averaged mistagging rate,  $m$ , are measured also from simulation for each  $n_{\text{jet}}$  and  $H_T$  bin, with both quantities averaged over jet  $p_T$  and  $\eta$ . Corrections are applied to both  $\epsilon$  and  $m$  in order to match the corresponding measurements with data [37, 38]. The aforementioned information is sufficient to determine an accurate prediction for  $n_b^{\text{reco}}$ . For example, an estimate for the number of events with zero reconstructed b-quark jets is given by the expression:

$$n_0^{\text{reco}} = \sum_{n_b \geq 0, n_q \geq 0} N(n_b, n_q) \times (1 - \epsilon)^{n_b} \times (1 - m)^{n_q} \quad (3)$$

A similar treatment is used for the other b-quark jet multiplicity categories. The yields from simulation, as determined with the method described above, are found to be in good agreement with the yields obtained directly from the simulation. The method exploits the ability to make precise measurements of  $N(n_b, n_q)$ ,  $\epsilon$  and particularly  $m$ , which means that predicted event yields for a given b-quark jet category can be made with a higher statistical precision than obtained directly from simulation. A precise measurement of  $m$  is particularly important for events with  $n_b^{\text{reco}} \geq 3$ , which occurs in the SM because of the presence of mistagged

jets in the event. In this case, the largest background is  $t\bar{t}$ , with two correctly tagged b-quark jets and an additional mistagged jet. Any contributions due to jets originating from bottom quarks in the event that might not be modelled correctly in the simulation are accounted for by measurements made in the  $\mu + \text{jets}$  sample.

Any mismodelling in the simulation of the event kinematics or instrumental effects observed in data are expected to largely cancel in the ratio of yields used to construct the translation factors, given that the data control and signal samples, and the corresponding event samples from simulation, are defined to be kinematically similar. However, a systematic uncertainty is assigned to each translation factor to account for theoretical uncertainties [43] and residual biases in the simulation modelling [11]. The magnitudes of the systematic uncertainties are determined from a representative set of closure tests in data, in which yields from one of the three independent control samples, along with the corresponding translation factors obtained from simulation, are used to predict the yields in another control sample, following the same prescription defined in Equation 2. The contamination from multijet events and any potential signal is expected to be negligible. Therefore, the closure tests carried out between control samples probe the properties of the relevant SM backgrounds.

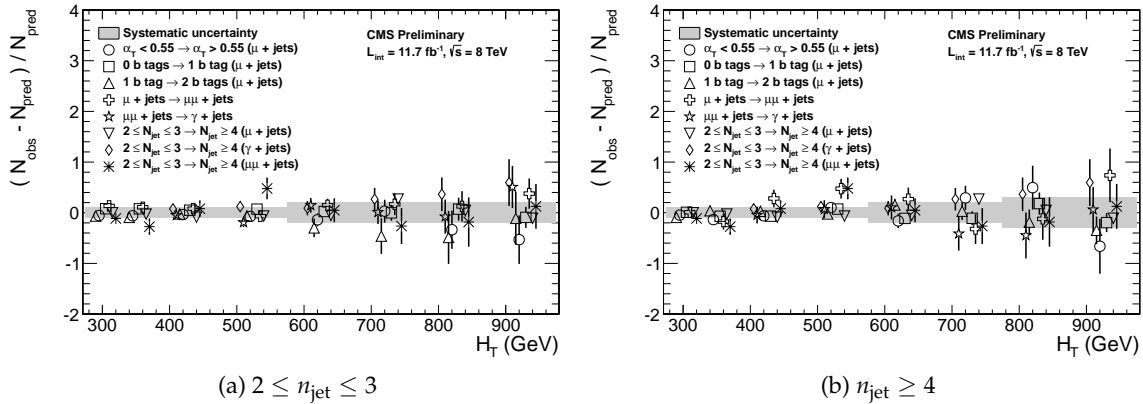


Figure 1: A set of closure tests split into the two jet multiplicity bins overlaid on top of grey bands that represent the systematic uncertainties used for the five  $H_T$  regions in the final simultaneous fit.

A set of eight closure tests, which probe key ingredients of the simulation modelling that may introduce biases to the translation factors, and the  $H_T$ -dependent systematic uncertainties are shown in Fig. 1. These sets of closure tests are repeated independently for the two exclusive jet multiplicity bins. The first three sets of closure tests are carried out within the  $\mu + \text{jets}$  sample, and probe the modelling of the  $\alpha_T$  distribution in genuine  $\ell_T$  events (circles), the relative composition between  $W + \text{jets}$  and top events (squares), and the modelling of the reconstruction of b-quark jets (triangles), respectively. The fourth set (crosses), connecting the  $\mu + \text{jets}$  and  $\mu\mu + \text{jets}$  control samples, addresses the modelling of the relative contributions of  $Z + \text{jets}$  to  $W + \text{jets}$  and top events while the fifth set (stars) deals with the consistency between the  $Z \rightarrow \mu\mu + \text{jets}$  and  $\gamma + \text{jets}$  samples. Furthermore, three additional sets of closure tests, one for each control sample, probe the simulation modelling of the  $n_{\text{jet}}$  distribution.

All individual closure tests demonstrate, within the statistical precision of each test, that there are no significant biases inherent in the translation factors obtained from simulation. The level of closure achieved in these tests is used to determine systematic uncertainties that are assigned to the translation factors. For each of the five regions  $275 < H_T < 325$  GeV,  $325 < H_T <$

$375 \text{ GeV}$ ,  $375 < H_T < 575 \text{ GeV}$ ,  $575 < H_T < 775 \text{ GeV}$  and  $H_T > 775 \text{ GeV}$ , independent systematic uncertainties are defined by the weighted sample variance of the closure tests found in each  $H_T$  region. This conservative procedure yields estimates of 10%, 10%, 10%, 20% and 20%, and 10%, 10%, 10%, 20% and 30%, for the five  $H_T$  regions defined above in the  $2 \leq n_{\text{jet}} \leq 3$  and  $n_{\text{jet}} \geq 4$  bins respectively. Uncertainties related to the modelling of b-quark jets in simulation are found to be negligible in comparison to the aforementioned uncertainties after corrections are applied to the efficiency and mis-tagging rates of b-quark jets obtained from simulation, in order to account for residual differences with respect to measurements in data.

## 6 Results

For a given category of events satisfying requirements on both  $n_{\text{jet}}$  and  $n_b^{\text{reco}}$ , a binned likelihood fit using all four data samples is carried out to obtain a consistent prediction of the SM background:

$$L_{\text{total}} = L_{\text{hadronic}} \times L_{\mu+\text{jets}} \times L_{\mu\mu+\text{jets}} \times L_{\gamma+\text{jets}} \quad n_b^{\text{reco}} \leq 1 \quad (4)$$

$$L_{\text{total}} = L_{\text{hadronic}} \times L_{\mu+\text{jets}} \quad n_b^{\text{reco}} \geq 2 \quad (5)$$

where  $L_{\text{hadronic}}$  describes the yields in the eight  $H_T$  bins of the signal region when exactly  $n_b^{\text{reco}}$  b-quark jets are required. In each bin of  $H_T$ , the observation is modelled as Poisson-distributed about the sum of a SM expectation and a potential signal contribution. The components of this SM expectation are related to the expected yields in the control samples via translation factors derived from simulation, as described in Sec. 5.2. Signal contributions in each of the four data samples are considered, though the only significant contribution occurs in the signal region and not the control samples. The systematic uncertainties associated with the translations are accounted for with nuisance parameters, the measurements of which are treated as log-normally-distributed. Since for  $n_b^{\text{reco}} \geq 2$  the dominant SM background arises from top events, only the  $\mu + \text{jets}$  control sample is used in the likelihood to determine the total contribution from all (non-multijet) SM backgrounds in the signal region.

In addition, any potential contribution from the multijet background in the signal region is estimated by exploiting the  $H_T$  dependence of the ratio of events that result in a value of  $\alpha_T$  above and below some threshold value. This dependence on  $H_T$  is modelled as a falling exponential function,  $Ae^{-kH_T}$  [12]. The parameters  $A$  and  $k$  are the normalisation and exponential decay constants, respectively. Values of  $A$  and  $k$  are determined by the fit independently for each category of reconstructed b-quark jets. The value of  $k$  is constrained via measurements in a multijet-enriched data side-band satisfying the criterion  $0.52 < \alpha_T < 0.55$ . A further side band, defined by inverting the  $H_T/\cancel{E}_T$  cleaning cut [12], is used to confirm that this method provides an unbiased estimator for  $k$  and to estimate a systematic uncertainty.

In order to test the compatibility of the observed yields with the expectations from SM processes only, the likelihood function is maximized over all fit parameters. A comparison of the observed yields and the SM expectations in bins of  $H_T$  for events with  $2 \leq n_{\text{jet}} \leq 3$  and exactly zero, one, or two reconstructed b-quark jets is shown in Figs. 2, 3, and 4, respectively. Similarly, the same comparison for events with  $n_{\text{jet}} \geq 4$  and zero, one, two, three, or at least four reconstructed b-quark jets is shown in Figs. 5, 6, 7, 8, and 9, respectively. For all eight  $(n_{\text{jet}}, n_b)$  categories, no significant excess above the SM expectation is observed in the signal region, and the control samples are well described by the SM hypothesis.

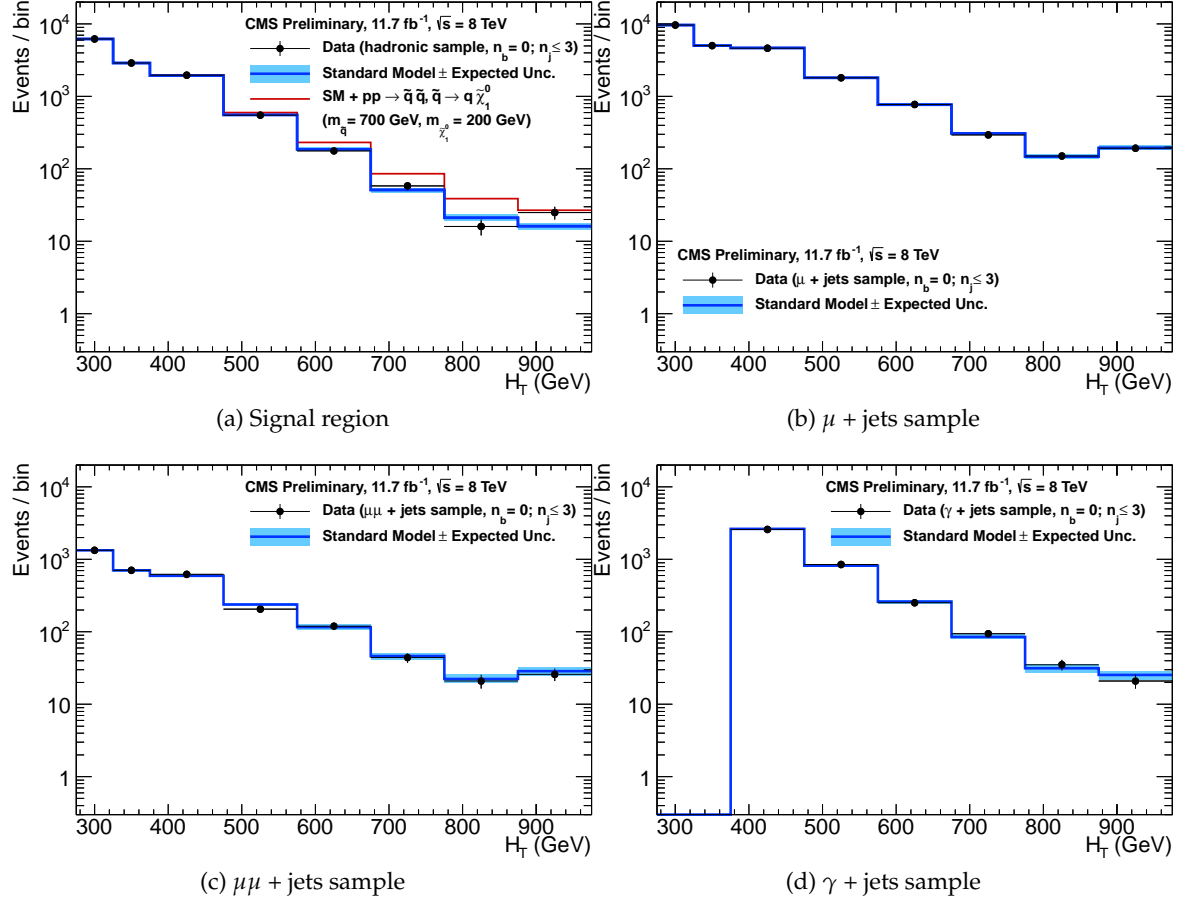


Figure 2: Comparison of the observed yields and SM expectations given by the simultaneous fit in bins of  $H_T$  for the (a) signal region, (b)  $\mu + \text{jets}$ , (c)  $\mu\mu + \text{jets}$  and (d)  $\gamma + \text{jets}$  control samples when requiring exactly zero reconstructed b-jets in the  $2 \leq n_{\text{jet}} \leq 3$  bin. The observed event yields in data (black dots) and the expectations and their uncertainties, as determined by the simultaneous fit, for all SM processes (dark blue solid line with light blue bands) are shown. For illustrative purposes only, the signal expectation (red solid line) for the model T2 with  $m_{\tilde{q}} = 700$  GeV and  $m_{\text{LSP}} = 200$  GeV is superimposed on the SM background expectation.

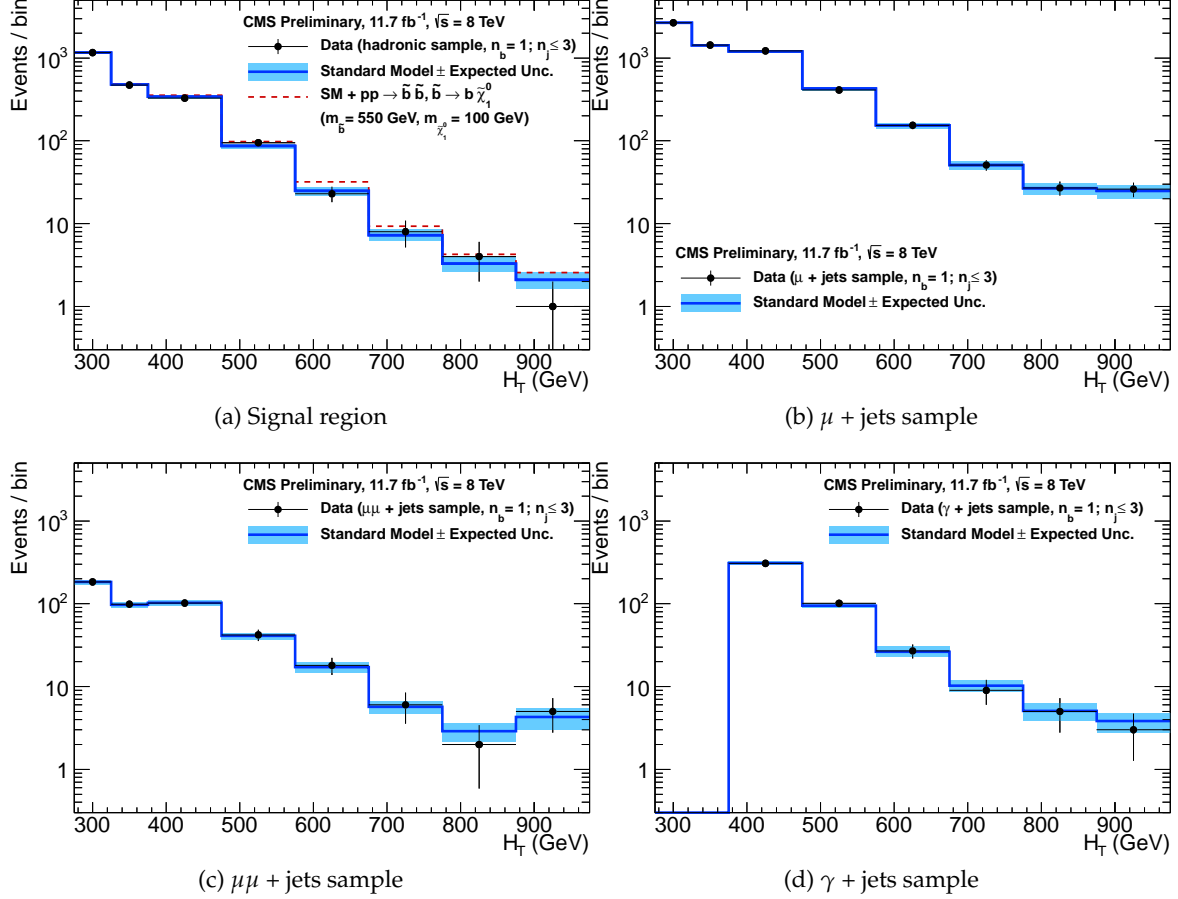


Figure 3: Comparison of the observed yields and SM expectations given by the simultaneous fit in bins of  $H_T$  for the (a) signal region, (b)  $\mu + \text{jets}$ , (c)  $\mu\mu + \text{jets}$  and (d)  $\gamma + \text{jets}$  control samples when requiring exactly one reconstructed b-jet in the  $2 \leq n_{\text{jet}} \leq 3$  bin. The observed event yields in data (black dots) and the expectations and their uncertainties, as determined by the simultaneous fit, for all SM processes (dark blue solid line with light blue bands) are shown. For illustrative purposes only, the signal expectation (red dashed line) for the model T2bb with  $m_{\tilde{b}} = 550 \text{ GeV}$  and  $m_{\text{LSP}} = 100 \text{ GeV}$  is superimposed on the SM background expectation.

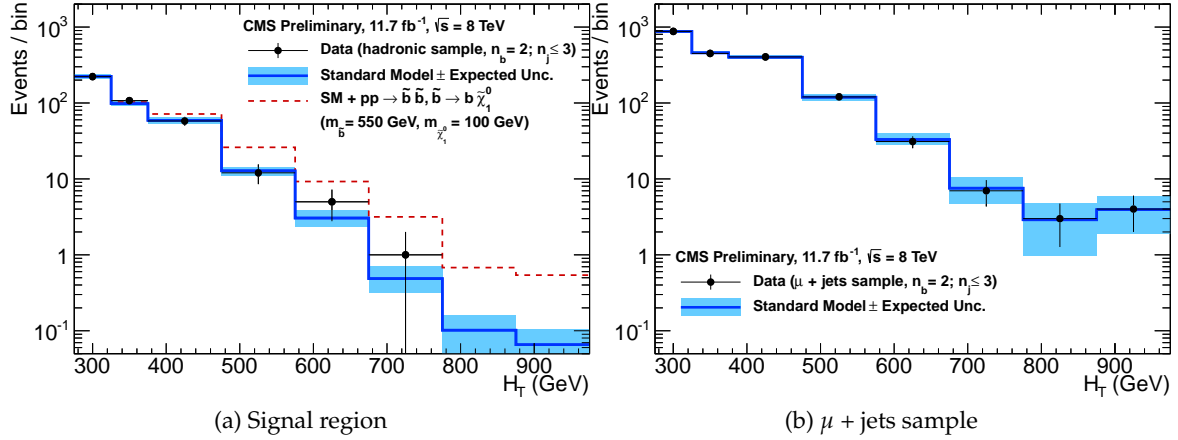


Figure 4: Comparison of the observed yields and SM expectations given by the simultaneous fit in bins of  $H_T$  for the (a) signal region and (b)  $\mu +$  jets control sample when requiring exactly two reconstructed b-jets in the  $2 \leq n_{jet} \leq 3$  bin. The observed event yields in data (black dots) and the expectations and their uncertainties, as determined by the simultaneous fit, for all SM processes (dark blue solid line with light blue bands) are shown. For illustrative purposes only, the signal expectation (red dashed line) for the model T2bb with  $m_{\tilde{b}} = 550$  GeV and  $m_{LSP} = 100$  GeV is superimposed on the SM background expectation.

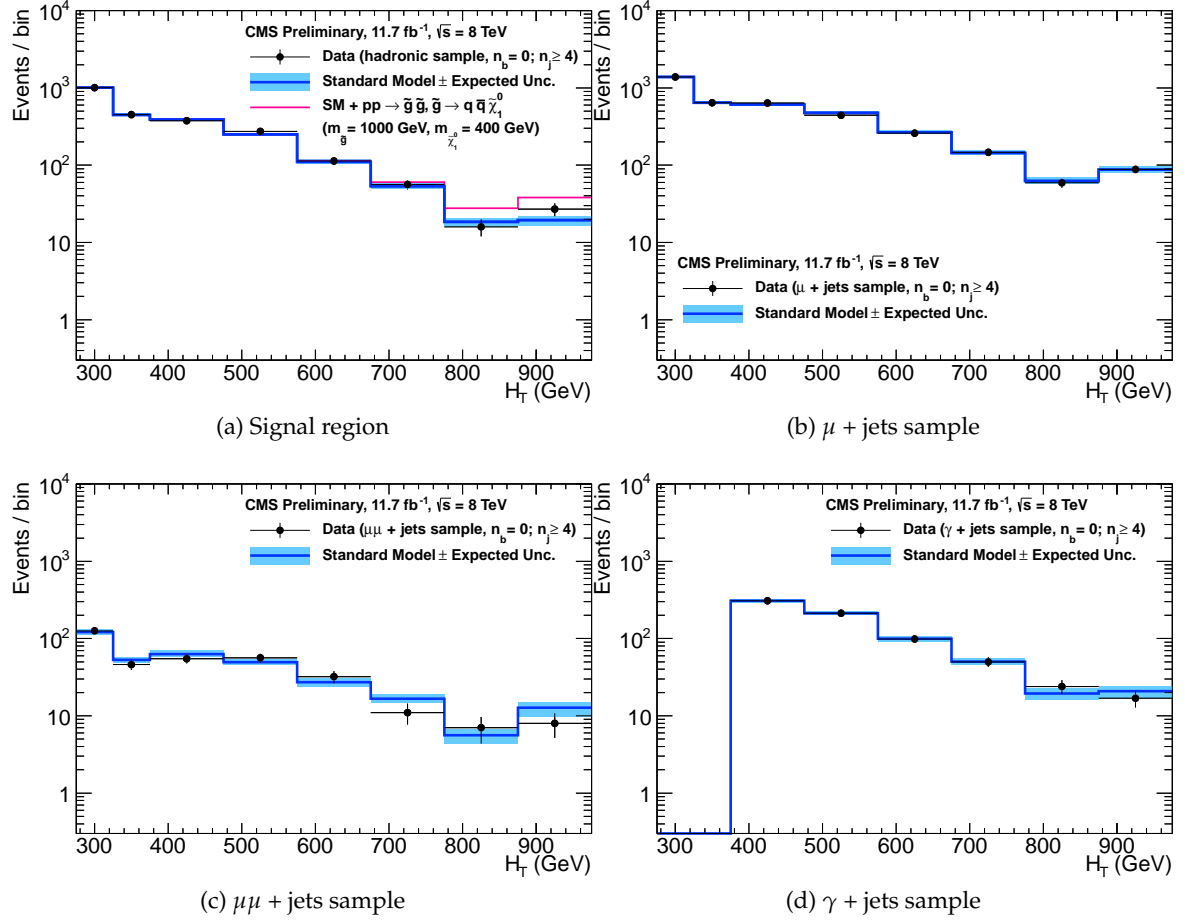


Figure 5: Comparison of the observed yields and SM expectations given by the simultaneous fit in bins of  $H_T$  for the (a) signal region, (b)  $\mu +$  jets, (c)  $\mu\mu +$  jets and (d)  $\gamma +$  jets control samples when requiring exactly zero reconstructed b-jets in the  $n_{jet} \geq 4$  bin. The observed event yields in data (black dots) and the expectations and their uncertainties, as determined by the simultaneous fit, for all SM processes (dark blue solid line with light blue bands) are shown. For illustrative purposes only, the signal expectation (magenta solid line) for the model T1 with  $m_g = 1000$  GeV and  $m_{LSP} = 400$  GeV is superimposed on the SM background expectation.

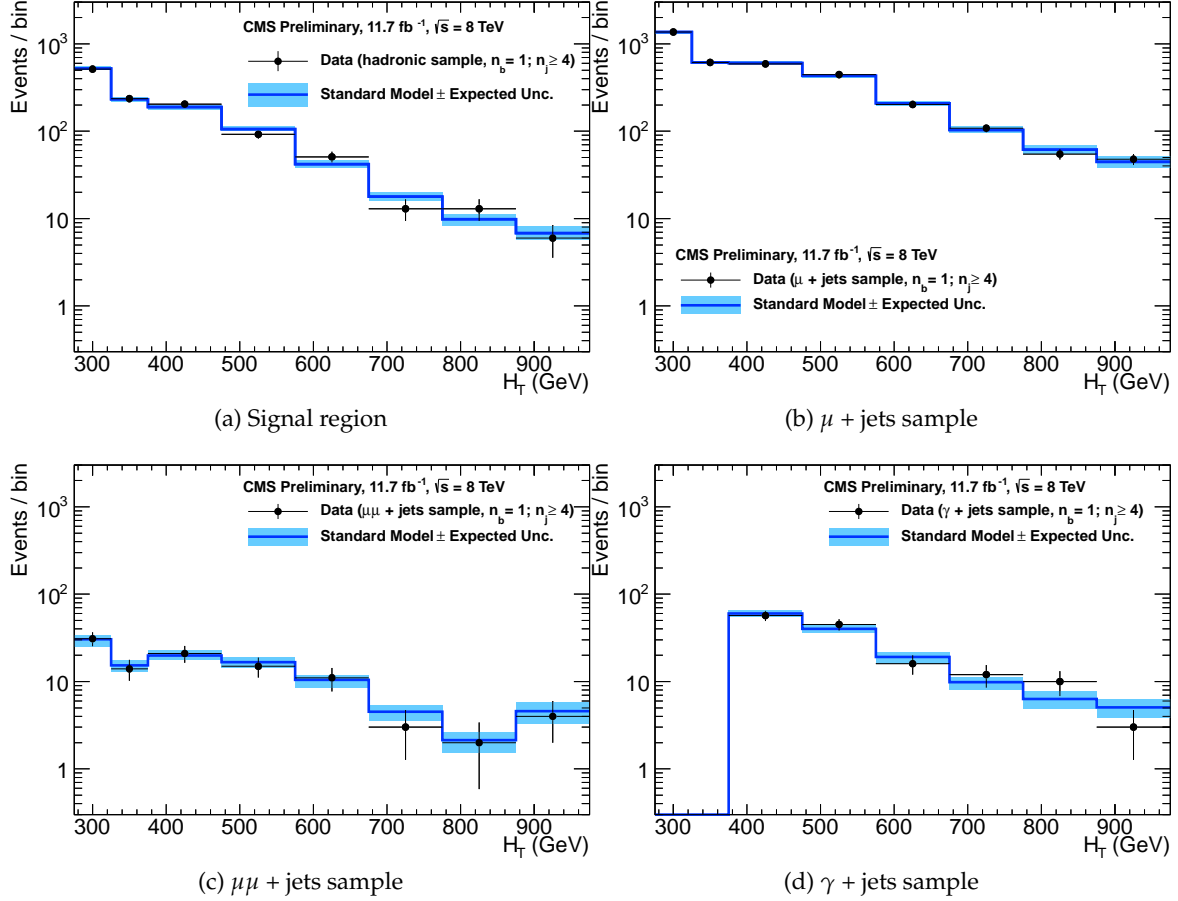


Figure 6: Comparison of the observed yields and SM expectations given by the simultaneous fit in bins of  $H_T$  for the (a) signal region, (b)  $\mu +$  jets, (c)  $\mu\mu +$  jets and (d)  $\gamma +$  jets control samples when requiring exactly one reconstructed b-jet in the  $n_{jet} \geq 4$  bin. The observed event yields in data (black dots) and the expectations and their uncertainties, as determined by the simultaneous fit, for all SM processes (dark blue solid line with light blue bands) are shown.

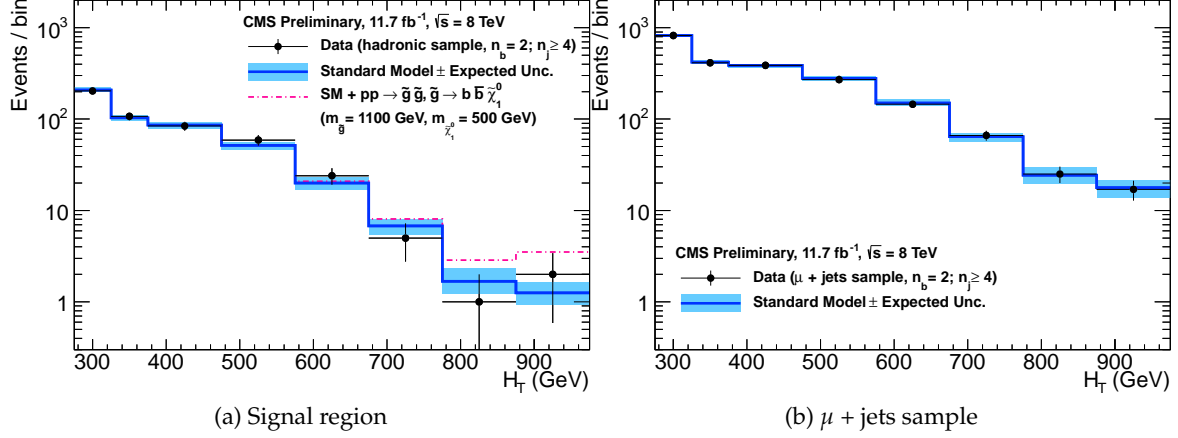


Figure 7: Comparison of the observed yields and SM expectations given by the simultaneous fit in bins of  $H_T$  for the (a) signal region and (b)  $\mu +$  jets control sample when requiring exactly two reconstructed b-jets in the  $n_{\text{jet}} \geq 4$  bin. The observed event yields in data (black dots) and the expectations and their uncertainties, as determined by the simultaneous fit, for all SM processes (dark blue solid line with light blue bands) are shown. For illustrative purposes only, the signal expectation (magenta dot-dashed line) for the model  $T1bbbb$  with  $m_{\tilde{g}} = 1100$  GeV and  $m_{LSP} = 500$  GeV is superimposed on the SM background expectation.

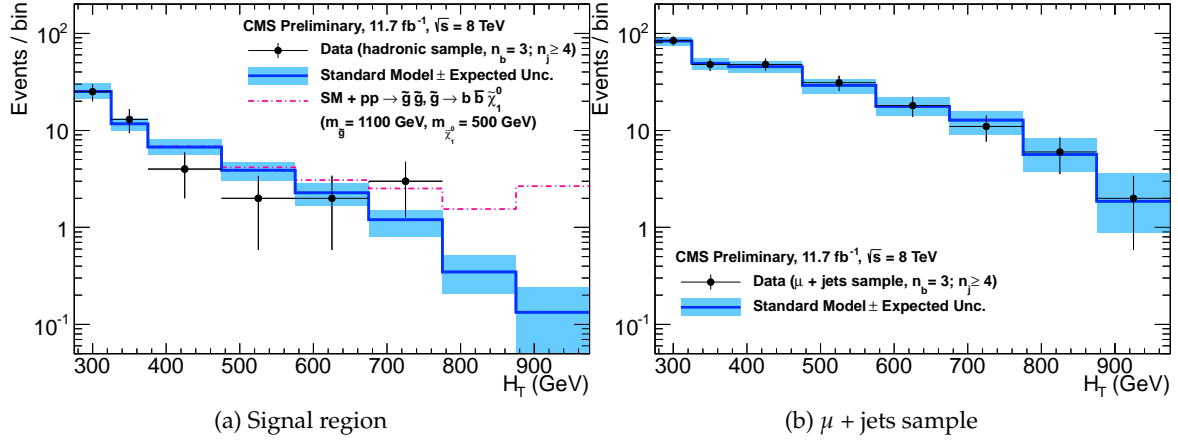


Figure 8: Comparison of the observed yields and SM expectations given by the simultaneous fit in bins of  $H_T$  for the (a) signal region and (b)  $\mu +$  jets control sample when requiring exactly three reconstructed  $b$ -jets in the  $n_{jet} \geq 4$  bin. The observed event yields in data (black dots) and the expectations and their uncertainties, as determined by the simultaneous fit, for all SM processes (dark blue solid line with light blue bands) are shown. For illustrative purposes only, the signal expectation (magenta dot-dashed line) for the model T1bbbb with  $m_{\tilde{g}} = 1100$  GeV and  $m_{LSP} = 500$  GeV is superimposed on the SM background expectation.

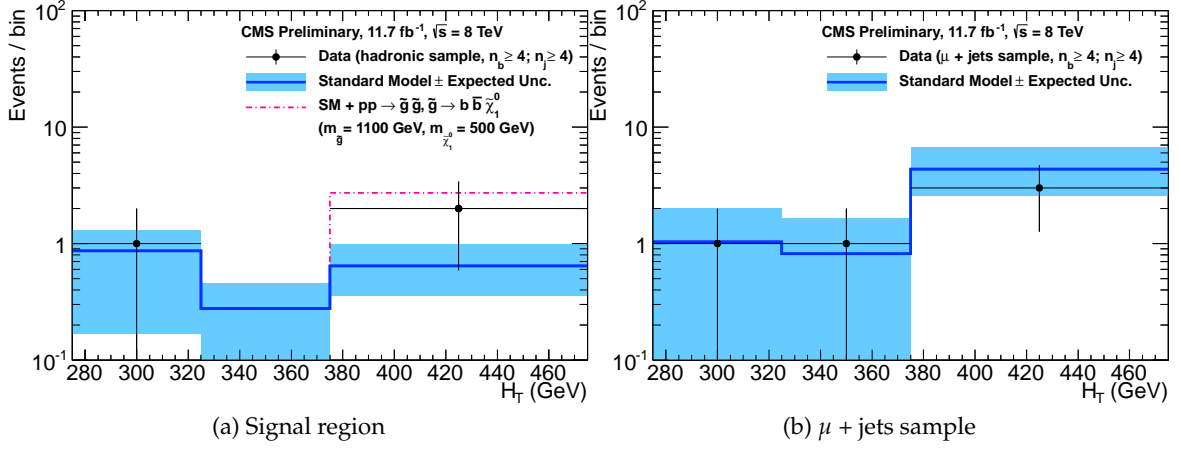


Figure 9: Comparison of the observed yields and SM expectations given by the simultaneous fit in bins of  $H_T$  for the (a) signal region and (b)  $\mu +$  jets control sample when requiring at least four reconstructed b-jets in the  $n_{\text{jet}} \geq 4$  bin. The observed event yields in data (black dots) and the expectations and their uncertainties, as determined by the simultaneous fit, for all SM processes (dark blue solid line with light blue bands) are shown. For illustrative purposes only, the signal expectation (magenta dot-dashed line) for the model T1bbbb with  $m_{\tilde{g}} = 1100$  GeV and  $m_{\tilde{\chi}_1^0} = 500$  GeV is superimposed on the SM background expectation.

## 7 Interpretation of the results

Limits are set in the parameter space of a set of simplified models that characterise both third-generation squark production and compressed spectra scenarios, where the mass difference between the primary produced sparticle (e.g. a squark or a gluino) and the LSP is rather small. The  $CL_s$  method [44, 45] is used to compute the limits, with the one-sided profile likelihood ratio as the test statistic [46]. The sampling distributions for the test statistic are built by generating pseudo-data from the likelihood function, using the respective maximum-likelihood values of the nuisance parameters under the background-only and signal-plus-background hypotheses.

Events samples for the simplified models are generated at leading order with PYTHIA 6.4 [47]. Inclusive, process-dependent, next-to-leading order calculations with next-to-leading logarithmic corrections [48] (NLO+NLL) of SUSY production cross sections are obtained with the program PROSPINO [49] and CTEQ6M [50] parton distribution functions. The simulated signal events include multiple interactions per LHC bunch crossing (pileup) with the distribution of reconstructed vertices that match the one observed in data.

The production and decay modes of the simplified models under consideration are summarised in Table 1. The models T1 and T2 are used to characterise the pair production of gluinos and first- or second-generation squarks, respectively, depending on their mass as well as on the LSP mass. The simplified models T2bb, T1tttt, and T1bbbb describe various production and decay mechanisms in the context of third-generation squarks.

Experimental uncertainties on the SM background predictions (10 – 30%), the luminosity measurement (4.4%), and the total acceptance times efficiency of the selection for the considered signal model (12%–23%) are included in the calculation of the limit. Signal efficiency in the kinematic region defined by  $0 < m_{\tilde{g}(\tilde{q})} - m_{\text{LSP}} < 175 \text{ GeV}$  or  $m_{\tilde{g}(\tilde{q})} < 300 \text{ GeV}$  is due in part to the presence of initial-state radiation. Given the large associated uncertainties, no interpretation is provided for this kinematic region. In the case of model T1tttt, for which pair-produced gluinos decay to  $t\bar{t}$  pairs and the LSP, the region  $0 < m_{\tilde{g}} - m_{\text{LSP}} < 400 \text{ GeV}$  is not considered.

Table 1: The first two columns specify the model and its production and decay. The next two columns specify the  $n_{\text{jet}}$  and  $n_b$  bins that are considered for each interpretation. The last two columns indicate the search sensitivity for each model, where  $m_{\tilde{q}(\tilde{g})}^{\text{best}}$  and  $m_{\text{LSP}}^{\text{best}}$  represent the largest mass beyond which no limit can be set for squarks (gluinos) and the LSP, respectively. The exclusion range for  $m_{\tilde{q}(\tilde{g})}$  is bounded from below by the kinematic region considered for each model, as defined in the text. The quoted estimates are determined conservatively from the observed exclusion based on the theoretical production cross section minus  $1\sigma$  uncertainty.

Model	Production/decay	$n_{\text{jet}}$	$n_b$	Limit plot	$m_{\tilde{q}(\tilde{g})}^{\text{best}}$ (GeV)	$m_{\text{LSP}}^{\text{best}}$ (GeV)
T1	$\text{pp} \rightarrow \tilde{g}\tilde{g} \rightarrow q\tilde{q}\tilde{\chi}^0 q\tilde{q}\tilde{\chi}^0$	$\geq 4$	0	10a	$\approx 950$	$\approx 450$
T2	$\text{pp} \rightarrow \tilde{q}\tilde{q} \rightarrow q\tilde{\chi}^0 \bar{q}\tilde{\chi}^0$	2–3	0	10b	$\approx 775$	$\approx 325$
T2bb	$\text{pp} \rightarrow b\bar{b} \rightarrow b\tilde{\chi}^0 b\tilde{\chi}^0$	2–3	1,2	10c	$\approx 600$	$\approx 200$
T1tttt	$\text{pp} \rightarrow \tilde{g}\tilde{g} \rightarrow t\bar{t}\tilde{\chi}^0 t\bar{t}\tilde{\chi}^0$	$\geq 4$	2,3, $\geq 4$	10d	$\approx 975$	$\approx 325$
T1bbbb	$\text{pp} \rightarrow \tilde{g}\tilde{g} \rightarrow b\bar{b}\tilde{\chi}^0 b\bar{b}\tilde{\chi}^0$	$\geq 4$	2,3, $\geq 4$	10e	$\approx 1125$	$\approx 650$

Figure 10 shows the upper limit on the cross section at 95% CL as a function of  $m_{\tilde{q}}$  or  $m_{\tilde{g}}$  and  $m_{\text{LSP}}$  for various simplified models. The point-to-point fluctuations are due to the finite number of pseudo-experiments used to determine the observed upper limit. The solid thick black line indicates the observed exclusion region assuming NLO+NLL [48, 49] SUSY cross section for

squark pair production in the limit of very massive gluinos (or vice versa). The thin black lines represent the observed excluded region when varying the cross section by its theoretical uncertainty. The dashed purple lines indicate the median (thick line)  $\pm 1\sigma$  (thin lines) expected exclusion regions.

The estimates on mass limits are determined conservatively from the observed exclusion based on the theoretical production cross section minus  $1\sigma$  uncertainty. The most stringent mass limits on pair-produced sparticles are obtained at low LSP masses, while the limits typically weaken for compressed spectra, i.e., points close to the diagonal. In particular, for all of the considered simplified models, there is an LSP mass beyond which no limit can be set. This is illustrated in Figure 10a, where the most stringent limit on the gluino mass of 950 GeV is obtained for low LSP masses. This limit only weakens to 900 GeV when the LSP mass reaches 425 GeV. However, for LSP masses above 450 GeV, no mass range can be excluded for gluinos decaying to first- or second-generation quarks. Table 1 summarises the mass limits obtained from the considered simplified models.

## 8 Summary

A search for supersymmetry is reported, based on a data sample of  $pp$  collisions collected at  $\sqrt{s} = 7$  TeV, corresponding to an integrated luminosity of  $11.7 \pm 0.5 \text{ fb}^{-1}$ . Final states with two or more jets and significant  $\cancel{E}_T$ , as expected from high-mass squark and gluino production and decays, have been analysed. An exclusive search has been performed in a binned signal region defined by the number of reconstructed jets, the scalar sum of the transverse energy of jets,  $H_T$ , and the number of jets identified to originate from a bottom quark. The sum of standard model backgrounds per bin has been estimated from a simultaneous binned likelihood fit to hadronic,  $\mu + \text{jets}$ ,  $\mu\mu + \text{jets}$ , and  $\gamma + \text{jets}$  samples. The observed yields are found to be in agreement with the expected contributions from standard model processes. Limits are set in simplified models, with a special emphasis on third generation squarks and compressed spectra scenarios. In the considered models with gluino pair production and for small LSP masses, exclusion limits of the gluino mass are in the range 950–1125 GeV. For simplified models with squark pair production, first or second generation squarks are excluded up to around 775 GeV and bottom squarks are excluded up to 600 GeV, again for small LSP masses. Thus, for the simplified models under consideration, the most constraining limits on the LSP and third-generation squark masses indicate that a large range of SUSY parameter space is yet to be probed by the LHC.

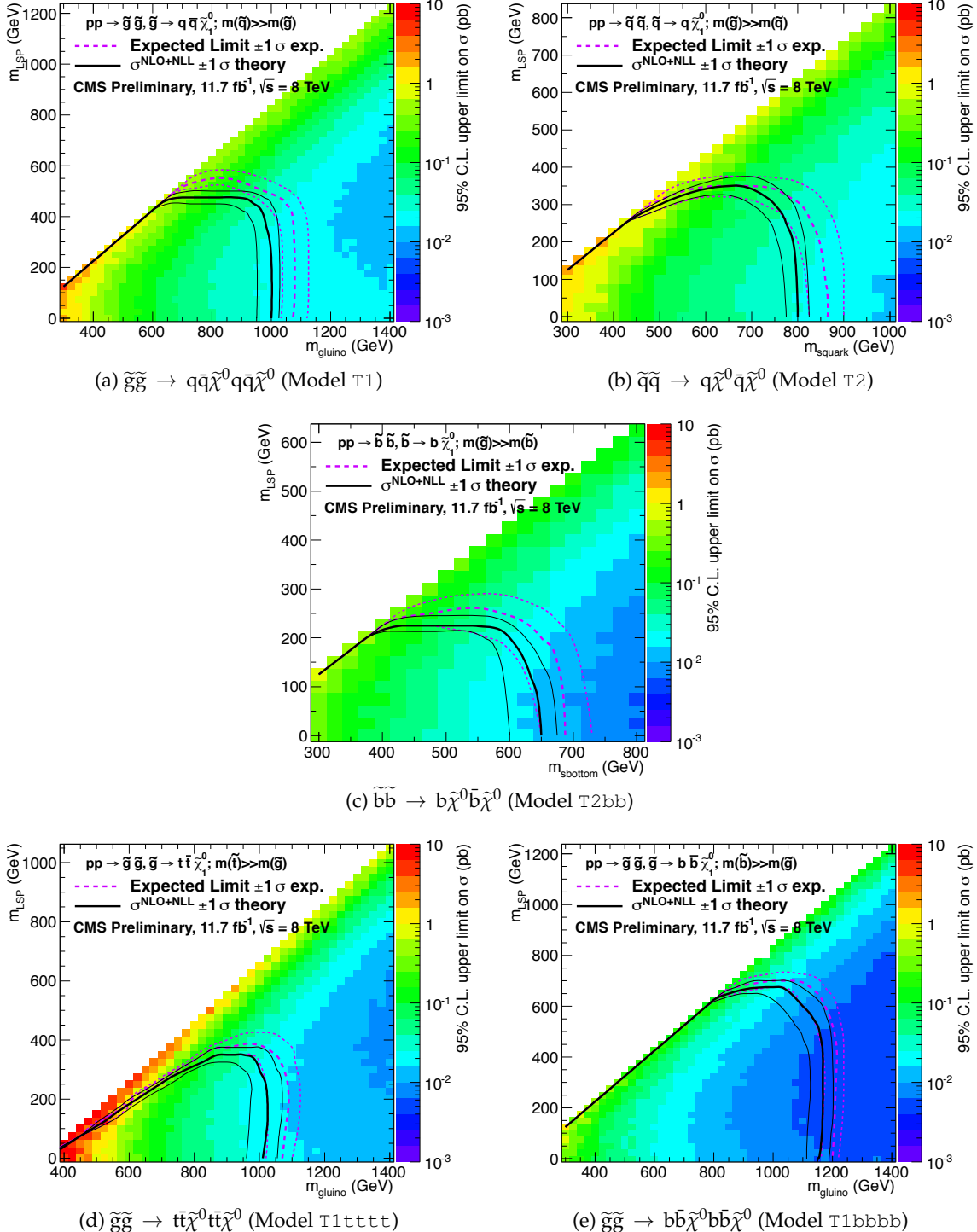


Figure 10: Upper limit on cross section at 95% CL as a function of  $m_{\tilde{q}}$  or  $m_{\tilde{g}}$  and  $m_{\text{LSP}}$  for various simplified models. The solid thick black line indicates the observed exclusion region assuming NLO+NLL SUSY production cross section. The thin black lines represent the observed excluded region when varying the cross section by its theoretical uncertainty. The dashed purple lines indicate the median (thick line)  $\pm 1\sigma$  (thin lines) expected exclusion regions.

## 9 Acknowledgements

We congratulate our colleagues in the CERN accelerator departments for the excellent performance of the LHC and thank the technical and administrative staffs at CERN and at other CMS institutes for their contributions to the success of the CMS effort. In addition, we gratefully acknowledge the computing centres and personnel of the Worldwide LHC Computing Grid for delivering so effectively the computing infrastructure essential to our analyses. Finally, we acknowledge the enduring support for the construction and operation of the LHC and the CMS detector provided by the following funding agencies: the Austrian Federal Ministry of Science and Research; the Belgian Fonds de la Recherche Scientifique, and Fonds voor Wetenschappelijk Onderzoek; the Brazilian Funding Agencies (CNPq, CAPES, FAPERJ, and FAPESP); the Bulgarian Ministry of Education, Youth and Science; CERN; the Chinese Academy of Sciences, Ministry of Science and Technology, and National Natural Science Foundation of China; the Colombian Funding Agency (COLCIENCIAS); the Croatian Ministry of Science, Education and Sport; the Research Promotion Foundation, Cyprus; the Ministry of Education and Research, Recurrent financing contract SF0690030s09 and European Regional Development Fund, Estonia; the Academy of Finland, Finnish Ministry of Education and Culture, and Helsinki Institute of Physics; the Institut National de Physique Nucléaire et de Physique des Particules / CNRS, and Commissariat à l'Énergie Atomique et aux Énergies Alternatives / CEA, France; the Bundesministerium für Bildung und Forschung, Deutsche Forschungsgemeinschaft, and Helmholtz-Gemeinschaft Deutscher Forschungszentren, Germany; the General Secretariat for Research and Technology, Greece; the National Scientific Research Foundation, and National Office for Research and Technology, Hungary; the Department of Atomic Energy and the Department of Science and Technology, India; the Institute for Studies in Theoretical Physics and Mathematics, Iran; the Science Foundation, Ireland; the Istituto Nazionale di Fisica Nucleare, Italy; the Korean Ministry of Education, Science and Technology and the World Class University program of NRF, Korea; the Lithuanian Academy of Sciences; the Mexican Funding Agencies (CINVESTAV, CONACYT, SEP, and UASLP-FAI); the Ministry of Science and Innovation, New Zealand; the Pakistan Atomic Energy Commission; the Ministry of Science and Higher Education and the National Science Centre, Poland; the Fundação para a Ciência e a Tecnologia, Portugal; JINR (Armenia, Belarus, Georgia, Ukraine, Uzbekistan); the Ministry of Education and Science of the Russian Federation, the Federal Agency of Atomic Energy of the Russian Federation, Russian Academy of Sciences, and the Russian Foundation for Basic Research; the Ministry of Science and Technological Development of Serbia; the Secretaría de Estado de Investigación, Desarrollo e Innovación and Programa Consolider-Ingenio 2010, Spain; the Swiss Funding Agencies (ETH Board, ETH Zurich, PSI, SNF, UniZH, Canton Zurich, and SER); the National Science Council, Taipei; the Thailand Center of Excellence in Physics, the Institute for the Promotion of Teaching Science and Technology and National Electronics and Computer Technology Center; the Scientific and Technical Research Council of Turkey, and Turkish Atomic Energy Authority; the Science and Technology Facilities Council, UK; the US Department of Energy, and the US National Science Foundation. Individuals have received support from the Marie-Curie programme and the European Research Council (European Union); the Leventis Foundation; the A. P. Sloan Foundation; the Alexander von Humboldt Foundation; the Belgian Federal Science Policy Office; the Fonds pour la Formation à la Recherche dans l'Industrie et dans l'Agriculture (FRIA-Belgium); the Agentschap voor Innovatie door Wetenschap en Technologie (IWT-Belgium); the Ministry of Education, Youth and Sports (MEYS) of Czech Republic; the Council of Science and Industrial Research, India; the Compagnia di San Paolo (Torino); and the HOMING PLUS programme of Foundation for Polish Science, cofinanced from European Union, Regional Development Fund.

## References

- [1] Y. A. Gol'fand and E. P. Likhtman, "Extension of the Algebra of Poincaré Group Generators and Violation of  $p$  Invariance", *JETP Lett.* **13** (1971) 323.
- [2] J. Wess and B. Zumino, "Supergauge transformations in four dimensions", *Nucl. Phys. B* **70** (1974) 39, doi:10.1016/0550-3213(74)90355-1.
- [3] H. P. Nilles, "Supersymmetry, Supergravity and Particle Physics", *Phys. Reports* **110** (1984) 1, doi:10.1016/0370-1573(84)90008-5.
- [4] H. Haber and G. Kane, "The Search for Supersymmetry: Probing Physics Beyond the Standard Model", *Phys. Reports* **117** (1987) 75, doi:10.1016/0370-1573(85)90051-1.
- [5] R. Barbieri, S. Ferrara, and C. A. Savoy, "Gauge Models with Spontaneously Broken Local Supersymmetry", *Phys. Lett. B* **119** (1982) 343, doi:10.1016/0370-2693(82)90685-2.
- [6] S. Dawson, E. Eichten, and C. Quigg, "Search for Supersymmetric Particles in Hadron - Hadron Collisions", *Phys. Rev. D* **31** (1985) 1581, doi:10.1103/PhysRevD.31.1581.
- [7] E. Witten, "Dynamical Breaking of Supersymmetry", *Nucl. Phys. B* **188** (1981) 513, doi:10.1016/0550-3213(81)90006-7.
- [8] S. Dimopoulos and H. Georgi, "Softly Broken Supersymmetry and  $SU(5)$ ", *Nucl. Phys. B* **193** (1981) 150, doi:10.1016/0550-3213(81)90522-8.
- [9] G. R. Farrar and P. Fayet, "Phenomenology of the Production, Decay, and Detection of New Hadronic States Associated with Supersymmetry", *Phys. Lett. B* **76** (1978) 575, doi:10.1016/0370-2693(78)90858-4.
- [10] CMS Collaboration, "Search for supersymmetry in final states with missing transverse energy and 0, 1, 2, or  $\geq 3$  b jets in 7 TeV pp collisions", (2012). arXiv:1210.8115. Submitted to JHEP.
- [11] CMS Collaboration, "Search for Supersymmetry at the LHC in Events with Jets and Missing Transverse Energy", *Phys. Rev. Lett.* **107** (2011) 221804, doi:10.1103/PhysRevLett.107.221804.
- [12] CMS Collaboration, "Search for Supersymmetry in pp Collisions at 7 TeV in Events with Jets and Missing Transverse Energy", *Phys. Lett. B* **698** (2011) 196, doi:10.1016/j.physletb.2011.03.021.
- [13] CMS Collaboration, "Search for new physics with jets and missing transverse momentum in pp collisions at  $\sqrt{s} = 7$  TeV", *JHEP* **08** (2011) 155, doi:10.1007/JHEP08(2011)155.
- [14] CMS Collaboration, "Inclusive search for squarks and gluinos in pp collisions at  $\sqrt{s} = 7$  TeV", *Phys. Rev. D* **85** (2012) 012004, doi:10.1103/PhysRevD.85.012004.
- [15] CMS Collaboration, "Search for supersymmetry in events with b jets and missing transverse momentum at the LHC", *JHEP* **07** (2011) 113, doi:10.1007/JHEP07(2011)113.

- [16] ATLAS Collaboration, “Search for squarks and gluinos using final states with jets and missing transverse momentum with the ATLAS detector in proton-proton collisions”, *Phys. Lett. B* **710** (2012) 67, doi:10.1016/j.physletb.2012.02.051.
- [17] ATLAS Collaboration, “Search for new phenomena in final states with large jet multiplicities and missing transverse momentum using  $\sqrt{s} = 7$  TeV pp collisions with the ATLAS detector”, *JHEP* **11** (2011) 099, doi:10.1007/JHEP11(2011)099.
- [18] ATLAS Collaboration, “Search for Scalar Bottom Quark Pair Production with the ATLAS Detector in  $pp$  Collisions at  $\sqrt{s} = 7$  TeV”, *Phys. Rev. Lett.* **108** (2012) 181802, doi:10.1103/PhysRevLett.108.181802.
- [19] ATLAS Collaboration, “Search for squarks and gluinos using final states with jets and missing transverse momentum with the ATLAS detector in proton-proton collisions”, *Phys. Lett. B* **701** (2011) 186, doi:10.1016/j.physletb.2011.05.061.
- [20] A. H. Chamseddine, R. Arnowitt, and P. Nath, “Locally Supersymmetric Grand Unification”, *Phys. Rev. Lett.* **49** (1982) 970, doi:10.1103/PhysRevLett.49.970.
- [21] R. Arnowitt and P. Nath, “Supersymmetric mass spectrum in SU(5) supergravity grand unification”, *Phys. Rev. Lett.* **69** (1992) 725, doi:10.1103/PhysRevLett.69.725.
- [22] G. L. Kane et al., “Study of constrained minimal supersymmetry”, *Phys. Rev. D* **49** (1994) 6173, doi:10.1103/PhysRevD.49.6173.
- [23] J. Alwall, P. Schuster, and N. Toro, “Simplified Models for a First Characterization of New Physics at the LHC”, *Phys. Rev. D* **79** (2009) 075020, doi:10.1103/PhysRevD.79.075020.
- [24] J. Alwall et al., “Model-Independent Jets plus Missing Energy Searches”, *Phys. Rev. D* **79** (2009) 015005, doi:10.1103/PhysRevD.79.015005.
- [25] D. Alves, N. Arkani-Hamed, S. Arora et al., “Simplified Models for LHC New Physics Searches”, arXiv:1105.2838. Official summary of results from the ‘Topologies for Early LHC Searches’ workshop, SLAC, September 2010.
- [26] CMS Collaboration, “Interpretation of Searches for Supersymmetry”, CMS Physics Analysis Summary SUS-11-016, (2012).
- [27] CMS Collaboration, “The CMS experiment at the CERN LHC”, *JINST* **03** (2008) S08004, doi:10.1088/1748-0221/3/08/S08004.
- [28] M. Cacciari, G. P. Salam, and G. Soyez, “The anti- $k_T$  jet clustering algorithm”, *JHEP* **04** (2008) 063, doi:10.1088/1126-6708/2008/04/063.
- [29] M. Cacciari and G. P. Salam, “Pileup subtraction using jet areas”, *Physics Letters B* **659** (2008) 119 – 126, doi:10.1016/j.physletb.2007.09.077.
- [30] M. Cacciari, G. P. Salam, and G. Soyez, “The catchment area of jets”, *Journal of High Energy Physics* **2008** (2008), no. 04, 005.
- [31] CMS Collaboration, “Determination of Jet Energy Calibration and Transverse Momentum Resolution in CMS”, *JINST* **6** (2011) P11002, doi:10.1088/1748-0221/6/11/P11002.

[32] CMS Collaboration, “Identification and filtering of uncharacteristic noise in the CMS hadron calorimeter”, *JINST* **5** (2010) T03014, doi:10.1088/1748-0221/5/03/T03014.

[33] CMS Collaboration, “Electromagnetic calorimeter commissioning and first results with 7 TeV data”, CMS Note CMS-NOTE-2010-012, (2010).

[34] CMS Collaboration, “Electron reconstruction and identification at  $\sqrt{s} = 7$  TeV”, CMS Physics Analysis Summary CMS-PAS-EGM-10-004, (2010).

[35] CMS Collaboration, “Performance of muon identification in pp collisions at  $\sqrt{s} = 7$  TeV”, CMS Physics Analysis Summary CMS-PAS-MUO-10-002, (2010).

[36] CMS Collaboration, “Isolated Photon Reconstruction and Identification at  $\sqrt{s} = 7$  TeV”, CMS Physics Analysis Summary CMS-PAS-EGM-10-006, (2010).

[37] CMS Collaboration, “b-Jet Identification in the CMS Experiment”, CMS Physics Analysis Summary CMS-PAS-BTV-11-004, (2012).

[38] CMS Collaboration, “Measurement of btagging efficiency using ttbar events”, CMS Physics Analysis Summary CMS-PAS-BTV-11-003, (2012).

[39] L. Randall and D. Tucker-Smith, “Dijet Searches for Supersymmetry at the Large Hadron Collider”, *Phys. Rev. Lett.* **101** (2008) 221803, doi:10.1103/PhysRevLett.101.221803.

[40] CMS Collaboration, “SUSY searches with dijet events”, CMS Physics Analysis Summary CMS-PAS-SUS-08-005, (2008).

[41] CMS Collaboration, “Search strategy for exclusive multi-jet events from supersymmetry at CMS”, CMS Physics Analysis Summary CMS-PAS-SUS-09-001, (2009).

[42] CMS Collaboration, “Data-Driven Estimation of the Invisible Z Background to the SUSY MET Plus Jets Search”, CMS Physics Analysis Summary SUS-08-002, (2008).

[43] Z. Bern et al., “Driving Missing Data at Next-to-Leading Order”, *Phys. Rev. D* **84** (2011) 114002, doi:10.1103/PhysRevD.84.114002.

[44] A. L. Read, “Presentation of search results: the CL s technique”, *J. Phys. G* **28** (2002) 2693, doi:10.1088/0954-3899/28/10/313.

[45] T. Junk, “Confidence level computation for combining searches with small statistics”, *Nucl. Instr. and Meth. A* **434** (1999) 435, doi:10.1016/S0168-9002(99)00498-2.

[46] G. Cowan et al., “Asymptotic formulae for likelihood-based tests of new physics”, *Eur. Phys. J. C* **71** (2011) 1554, doi:10.1140/epjc/s10052-011-1554-0.

[47] T. Sjöstrand, S. Mrenna and P. Z. Skands, “PYTHIA 6.4 Physics and Manual”, *JHEP* **05** (2006) 026, doi:10.1088/1126-6708/2006/05/026.

[48] M. Krämer et al., “Supersymmetry production cross sections in pp collisions at  $\sqrt{s} = 7$  TeV”, (2012). arXiv:1206.2892.

[49] W. Beenakker et al., “Squark and gluino production at hadron colliders”, *Nucl. Phys. B* **492** (1997) 51, doi:10.1016/S0550-3213(97)00084-9.

[50] J. Pumplin et al., “New generation of parton distributions with uncertainties from global QCD analysis”, *JHEP* **07** (2002) 012, doi:10.1088/1126-6708/2002/07/012.